Corrosion Science 122 (2017) 61–73

Contents lists available at ScienceDirect

Corrosion Science

journal homepage: www.elsevier.com/locate/corsci

Thermal oxidation of Ti-6Al–4V alloy and pure titanium under external bending strain: Experiment and modelling

Yang Zhang [a], Guo-Rong Ma [a], Xian-Cheng Zhang [a,*], Shaofan Li [b,*], Shan-Tung Tu [a]

[a] Key Laboratory of Pressure Systems and Safety, Ministry of Education, East China University of Science and Technology, Shanghai, PR China
[b] Department of Civil and Environmental Engineering, University of California at Berkeley, CA, USA

ARTICLE INFO

Article history:
Received 1 April 2016
Received in revised form 1 January 2017
Accepted 16 January 2017
Available online 19 January 2017

Keywords:
A. Titanium
C. Oxidation
C. Effects of strain
B. Modelling studies
B. X-ray diffraction
B. SEM

ABSTRACT

The thermal oxidation behaviour of Ti-6Al–4V alloy as well as pure titanium under external bending strains was investigated through experimental and modelling approaches. Dislocation accumulation due to creep deformation was responsible for the acceleration of oxidation at initial stage. However, the promoted formation of alumina would retard the subsequent scale growth. Moreover, the bending strain had a multi-fold influence on the formation of oxygen diffusion zone. An analytical model was developed to predict the variation of growth stress within the oxide layer along with time. The prediction results agreed well with experimental data.

1. Introduction

Owing to its excellent mechanical properties and corrosion resistance, Ti-6Al–4V alloy has been widely used in different industrial fields, including marine structure components, turbine engine blades and pressure vessels [1–4]. However, the poor thermal-oxidation resistance limited its applications at elevated temperatures. Moreover, the application of external loads made this situation more complicated because the external loads could significantly affect the oxidation behaviour of Ti-6Al–4V alloy [5].

A variety of research has been conducted to investigate the thermal oxidation behaviour of Ti-6Al–4V alloy [6–15]. When the alloy was exposed to an aggressive oxidizing environment, rutile nuclei would preferentially form on the alloy surface and then gradually cover the surface [6,8]. Meanwhile, outward diffusion of titanium and inward diffusion of oxygen would take place simultaneously [6,8,9]. The addition of vanadium would decrease the solubility of aluminum, prevent the formation of alumina at the oxide/substrate interface and promote the aluminum to diffuse outwards [6]. In the later oxidation stage, the inadequacy of activated titanium allowed more aluminium to diffuse outwards through the oxide layer [6]. Finally, nodular alumina became the favoured oxidation product at the gas/oxide interface [6]. Meanwhile, part of the oxygen atoms would diffuse and dissolve into the alloy substrate as interstitial atoms [6,8,9]. The absorption of oxygen into the underneath substrate promoted the phase transformation from beta-phase titanium to alpha-phase [11,13]. As a result, the oxygen diffusion zone (ODZ) would be formed underneath the oxide layer.

The research on the interaction between stress and oxidation can be mainly divided into two categories. The first category was to examine the origin and the development of growth stress during scale growth process. Many experiments have been carried out to measure the growth stress [16–19], and various theories were proposed to explain the generation of growth stress. The Pilling-Bedworth ratio (PBR), which was defined as the volume ratio between formed oxide and consumed metal, was once widely used to predict the sign of growth stress. It was generally believed that the oxide with larger volume was constrained by the underlying substrate when the value of PBR was higher than 1. It would result in the lattice mismatch between oxide and substrate and the generation of compressive stress within the oxide layer [20,21]. The growth strain was a time-dependent variable [16,22]. The linear relationship between growth strain and scale thickness was determined by Clarke et al. through describing the dislocations climb process during the diffusion of ions [22]. Following Clark's idea, a variety of analytical models were proposed to predict the evolution of growth stress along with time [23–27]. Among these models, the

* Corresponding authors.
E-mail addresses: xczhang@ecust.edu.cn (X.-C. Zhang), li@ce.berkeley.edu (S. Li).

http://dx.doi.org/10.1016/j.corsci.2017.01.009
0010-938X/

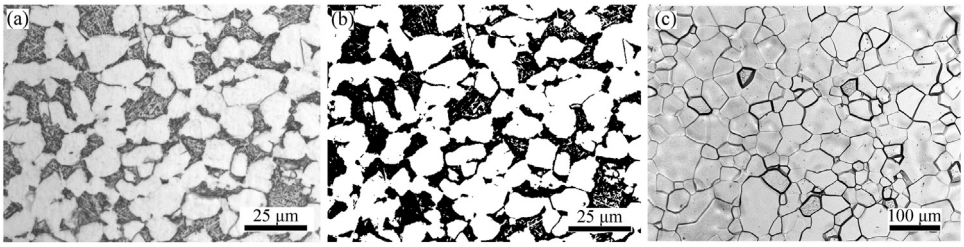

Fig. 1. (a) Cross-sectional microstructure of Ti-6Al-4V alloy, (b) binary image of Ti-6Al-4V microstructure, and (c) cross-sectional microstructure of pure titanium.

stress accumulation due to growth strain and its relaxation due to creep strain were considered by Maharjan et al. [24]. However, the additional component of growth strain due to ODZ has not been considered in the above analytical models. Meanwhile, if the oxidation kinetics is a piece-wise function of time, the constitutive equations should become much more complicated.

The second category was to investigate the effect of applied load on the oxidation behaviour. The main conclusions obtained from the available literature were controversial. It was generally believed that the tensile stress would accelerate the scale growth process. The formation of cracks in oxide layer due to tensile stress provided additional diffusion channels for the oxygen atoms [28,29]. However, the experimental results by Fargeix and Ghibaudo indicated that the formation of vacancies would promote the diffusion of elements through the oxide layer [30]. On the basis of Fick's law, Evans developed a model to describe the stress-dependent vacancy concentration [20], which was widely used in the subsequent research [31,32]. However, Irene et al. suggested that metals or alloys were always screened by previously formed oxide. Then the additionally compressive stress would increase the creep strain rate, leading to the removal of screening oxide and increment of reaction rate [33]. Moreover, the experimental results by Zhou et al. indicated that both externally tensile and compressive stresses would promote the nickel oxidation, and the compressive stress was more pronounced [34]. Hence, it can be concluded that the influence of external loads on oxidation products and kinetics has still not been clarified.

The aim of this paper was to investigate the thermal oxidation behaviour of Ti-6Al–4V alloy as well as pure titanium under external bending strains. The effect of external strains on the growth of oxide layer and ODZ was experimentally identified. Moreover, an analytical model was developed to predict the growth stress within the oxide layer.

2. Experimental procedure

2.1. Materials

The as-received Ti-6Al–4V alloy and pure titanium in the form of plate was provided by Baoji Titanium Industry CO., LTD, China. Prior to oxidation, the as-received plate of Ti-6Al–4V alloy was solution-treated for 1 h at 1073 K, and then annealed at 973 K for 2 h to relieve residual stress. The nominal chemical compositions (in wt.%) of Ti-6Al–4 V alloy were 5.87 Al, 4.04 V, 0.125 Fe, 0.022C, 0.17 O, 0.03 N, 0.01 Si and balanced Ti. The pure titanium was annealed at 823 K for 2 h to relieve residual stress. Chemical analysis showed the nominal chemical compositions (in wt.%) of pure titanium were 0.86C, 0.33 N, 0.3 O, 0.14 Si and balanced Ti. The cross-sectional microstructures of Ti-6Al–4V alloy and pure titanium were shown in Fig. 1. The Ti-6Al–4V alloy consisted of equiaxed primary α-grains and lamellar transformed β-grains. The pixel analysis of the binary image revealed that the area fractions of alpha phase and beta phase were respectively 67% and 33%, as seen in Fig. 1b. According to Delesse's equation, the volume fraction of a specific phase is approximately equal to its area fraction [35]. The pure titanium was entirely composed of alpha phase. The uniaxial tension testing results indicated that the yielding strength, ultimate strength, and Young's modulus of Ti-6Al–4V alloy were respectively 912.5 MPa, 980.6 MPa and 119.5 GPa, as shown in Fig. 2. For pure titanium, they were respectively 293.3 MPa, 219.8 MPa and 115.9 GPa.

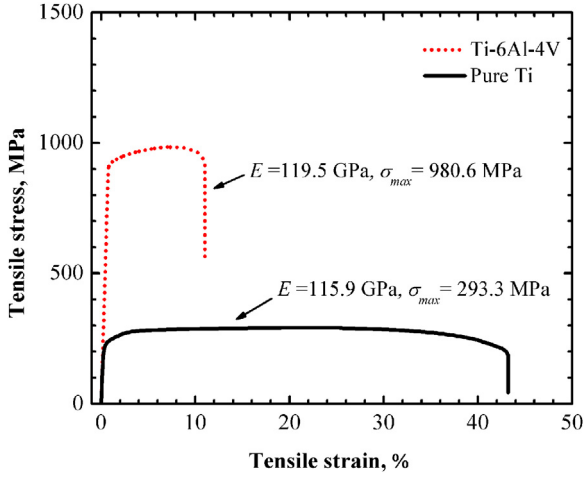

Fig. 2. Tensile stress-strain curves of Ti-6Al-4V alloy and pure titanium.

2.2. Oxidation experiments

Isothermal oxidation of Ti-6Al–4V alloy and pure titanium was conducted at 873 K for up to 96 h in air. The specimens used in oxidation experiments were cut into plates with the dimensions of $68 \times 30 \times 2\ mm^3$ by using wire electrical discharge cutting machine. The oxidation behaviour at the $68 \times 30\ mm^2$ surface was investigated. Before oxidation, the specimen surface was ground with 1200 grit SiC papers, and then cleaned ultrasonically in ethanol.

Bending strains were applied at the $68 \times 30\ mm^2$ surfaces to investigate the effect of external strains on the oxidation behaviour. The experimental set-up was designed according to ASTM G39-99 standard guideline [36], as shown in Fig. 3. The maximum deflection of specimens was kept to be 1 mm prior to oxidation experiments, which was monitored by a micrometre. The initial elastic strain, ε_0, was calculated according to the following equation [36],

$$\varepsilon_0 = 12hy\left(3H^2 - 4A^2\right)^{-1} \quad (1)$$

where h is the specimen thickness, y is the maximum deflection, H and A are the distance between outer supports and that between outer and inner supports. In the present work, h, H and A were respectively 2.0, 50.8 and 12.7 mm. Hence, the initial elastic strains were respectively 0.0034 and −0.0034 at the tensile and compres-

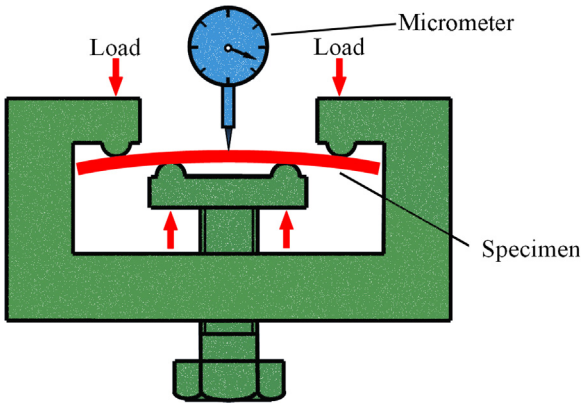

Fig. 3. Schematic showing the experimental set-up for oxidation.

sive surfaces of the loaded specimen. The oxidation experiment of unloaded specimens was also carried out for comparison.

2.3. Characterization of oxidation behaviour

The surface morphology of oxidized Ti-6Al–4V specimens were observed by a ZEISS EVO® MA 15 scanning electron microscope (SEM) equipped with energy dispersive spectrum (EDS). The XRD patterns of the oxidation products were recorded on a AXS D8-Advance apparatus using Cu Kα (λ = 1.54 Å) radiation with a step increment of 0.02°. The oxidation products of pure titanium were also determined for comparison. The residual stresses within the oxide layers were measured by $\sin^2\psi$ method. According to Bragg's law, the linear relationship between wavelength, λ, and lattice spacing, d^{hkl}, was used, i.e.,

$$\lambda = 2d^{hkl}\sin\theta^{hkl} \tag{2}$$

where θ^{hkl} is the diffraction angle. Then, the elastic strain of $\{hkl\}$ plane, ε_e^{hkl}, is calculated as

$$\varepsilon_e^{hkl} = \frac{1}{d_0^{hkl}}\left(d^{hkl} - d_0^{hkl}\right) \tag{3}$$

where d_0^{hkl} is the lattice space in a stress-free state. For a biaxial principal stress state, the stress, σ, can be expressed as [37]

$$\sigma = \varepsilon_e^{hkl}\left(2S_1 + \frac{1}{2}S_2\sin^2\psi\right)^{-1} \tag{4a}$$

$$S_1 = -\frac{1}{E_{ox}}\nu_{ox} \tag{4b}$$

$$S_2 = 2(1+\nu_{ox})\frac{1}{E_{ox}} \tag{4c}$$

where E_{ox} and ν_{ox} are respectively Young's modulus and Poisson's ratio of oxide layer. Härting et al. used the $\sin^2\psi$ method to measure the three-dimensional residual stress within naturally grown rutile layer on Ti-6Al–4V [38], where the parameters S_1 and S_2 were respectively determined to be -0.825×10^{-6} and $7.977\times10^{-6}\,mm^2/N$. In the present work, XRD pattern of rutile phase was chosen to measure the residual stress within oxide layers on Ti-6Al–4V and pure titanium. To avoid the interference from alumina, Bragg angle at 131.84° corresponding to (422) plane was selected.

The cross-sectional microstructures of the oxidized specimens were also observed by SEM. Prior to observation, the surfaces of the oxidized specimens were coated with thin nickel layer and then mounted in the epoxy resin. After grinding and polishing, etching treatment was conducted at room temperature for 15 s. The etchant was chosen as the mixture of 2% HF and 98% H_2O.

3. Modelling on growth stress

Fig. 4 shows the framework of the present model. Upon cooling to room temperature, thermal stress is inevitably generated. Residual stress is the superposition of growth stress and thermal stress. For the growth stress, it is the sum of intrinsic growth stress and stress generated during the scale growth process. Creep strain, elastic strain, growth strain and external strain contribute to the total strain. Clarke's model, Hook's law and Norton's law are respectively used to calculate the growth, elastic and creep strains. Growth strain is related to oxidation reaction at the interface and the diffusion of elements through the oxide layer. When the oxide layer is initially formed on the alloy surface, the lattice mismatch between oxide and substrate leads to the generation of intrinsic growth strain. Then, additional growth strain is induced by the dislocation climb through the oxide scale during the scale growth process.

3.1. Oxidation kinetics

The oxidation kinetics equation is generally given by [24]

$$h_{ox} = (K_{ox}t)^{\gamma} \tag{5}$$

where K_{ox} and γ are respectively the kinetics constant and index, and t is the oxidation time. Then the scale growth rate is obtained as

$$\frac{dh_{ox}}{dt} = K_{ox}\gamma\left(\frac{1}{h_{ox}}\right)^{\frac{1-\gamma}{\gamma}} \tag{6}$$

Considering that γ is in the range from 0 to 1, Eq. (6) is the general expression to describe the negative correlation between the oxide thickness and growth rate. Especially, when γ is equal to 0.5, Eq. (6) is simplified to Wagner's model, where the oxidation kinetics obeys a parabolic law. For the case of Ti-6Al–4V alloy, the oxidation product is composed of multiple components. Since the formation of alumina will obviously affect the oxidation kinetics, the oxidation process should be divided into two distinct stages [6]. If the piecewise point is assumed to be t_0, the scale growth rate can be expressed as

$$\frac{dh_{ox}}{dt} = \begin{cases} K_{ox1}\gamma_1\left(\frac{1}{h_{ox}}\right)^{\frac{1}{\gamma_1}(1-\gamma_1)} & (t \le t_0) \\ K_{ox2}\gamma_2\left(\frac{1}{h_{ox}}\right)^{\frac{1}{\gamma_2}(1-\gamma_2)} & (t > t_0) \end{cases} \tag{7}$$

where the subscripts 1 and 2 respectively denote the first and second oxidation stage. Then the modified kinetics equation can be expressed as

$$h_{ox} = \begin{cases} (K_{ox1}t)^{\gamma_1} & (t \le t_0) \\ \left[K_{ox2}(t-t_0) + (K_{ox1}t_0)^{\frac{1}{\gamma_2}\gamma_1}\right]^{\gamma_2} & (t > t_0) \end{cases} \tag{8}$$

3.2. Evolution of stress along with time

The thermal stress generated in the oxide layer during cooling process, σ_{th}, can be calculated using the following equation [32]

$$\sigma_{th} = \frac{E_{ox}}{1-\nu_{ox}}(\alpha_{ox} - \alpha_m)\,\Delta T \tag{9}$$

where α_{ox} and α_m are respectively the coefficients of thermal expansion (CTEs) of oxide and substrate, and ΔT is the temperature difference.

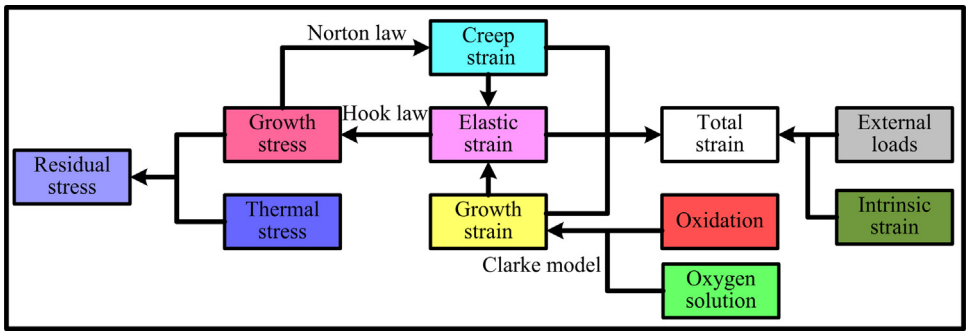

Fig. 4. Schematic showing the framework of the present model.

The total strain of the oxide, ε, is the sum of growth strain, ε_g, creep strain, ε_c, and elastic strain, ε_e, i.e.,

$$\varepsilon = \varepsilon_g + \varepsilon_c + \varepsilon_e \tag{10}$$

Under bending loads, the total strain of oxide depends on the curvature of the system. When the curvature is kept constant, the derivative of total strain with respect to time is zero, i.e.,

$$\frac{d\varepsilon}{dt} = \frac{d\varepsilon_g}{dt} + \frac{d\varepsilon_c}{dt} + \frac{d\varepsilon_e}{dt} = 0 \tag{11}$$

The elastic strain rate can be expressed as

$$\frac{d\varepsilon_e}{dt} = \frac{E_{ox}}{1-\nu_{ox}}\frac{d\sigma_g}{dt} \tag{12}$$

where σ_g is the growth stress within the oxide layer. Under a stationary creep condition, the creep strain rate can be expressed by Norton equation, i.e.,

$$\frac{d\varepsilon_c}{dt} = sgn(\sigma_g) \times B|\sigma_g|^m \tag{13}$$

where B and m are respectively the creep constant and index, and sgn$(\cdot)$ is the signal function which is defined as

$$sgn(x) = \begin{cases} +1, & (x>0) \\ 0, & (x=0) \\ -1, & (x<0) \end{cases} \tag{14}$$

According to Clarke's theory, when the dislocation climbs perpendicularly to the oxide/alloy interface, the volume change due to attachment of ions is responsible for the growth strain accumulation. The growth strain rate can be expressed as [22]

$$\frac{d\varepsilon_g}{dt} = \frac{1}{bda}\Omega\theta A_1 J_{c,\sigma} - \frac{1}{bda}\Omega\theta A_2 \exp\left(-E_T - \frac{1}{kT}\sigma_g \Delta\Omega\right) \tag{15}$$

where Ω, θ, b, d and a are respectively the volume of an oxide molecule, angle of symmetrical tilt boundary, Burgers vector, grain size and the average distance of traps, A_1 and A_2 are respectively related to the attachment and detachment of ions, $J_{c,\sigma}$, $\Delta\Omega$, and E_T respectively represent stress-assisted flux of ions, activation energy and trapping energy, k is Boltzmann's constant and T is Kelvin's temperature. The second term of Eq. (15) is often ignored due to its extremely small magnitude [22]. Clarke suggested that the compressive growth stress would be generated when the ions were attached by dislocations during diffusion. However, if the vacancy is trapped there, the dislocations would climb in the opposite direction and then tensile growth stress is generated. In Clarke's model, the flux is only related to the oxidation rate. However, the ODZ is inevitably formed during thermal oxidation of titanium alloy or pure titanium. Hence, the flux can be expressed as the sum of flux due to oxidation, J_{ox}, which is proportional to growth rate of oxide layer, and that due to oxygen solution, J_s, i.e.,

$$J_{c,\sigma} = J_{ox} + J_s \tag{16}$$

where J_{ox} can be calculated as

$$J_{ox} = \frac{1}{S}\frac{dN_{O_2}}{dt} \tag{17}$$

where S is the area of oxidized surface and N_{O_2} is the amount of diffused oxygen molecules due to oxidation. Due to the stoichiometric relationship, N_{O_2} is proportional to the amount of oxide, N_{MO_z}, i.e.,

$$N_{O_2} = \frac{1}{2}zN_{MO_z} \tag{18}$$

where z represents the stoichiometric number of metallic oxide MO_z. And N_{MO_z} is given by

$$N_{MO_z} = \frac{1}{V_{MO_z}}h_{ox}S \tag{19}$$

where V_{MO_z} is the molar volume of oxide. Substituting Eqs. (8), (18) and (19) into Eq. (17), J_{ox} can be expressed as

$$J_{ox} = \begin{cases} \frac{1}{2V_{MO_z}} z\gamma_1 K_{ox1}{}^{\gamma_1} t^{\gamma-1} & (t \le t_0) \\ \frac{1}{2V_{MO_z}} z\gamma_2 K_{ox2}\left[K_{ox2}(t-t_0) + (K_{ox1}t_0)^{\frac{1}{\gamma_2}\gamma_1}\right]^{\gamma_2-1} & (t > t_0) \end{cases} \tag{20}$$

The distribution of oxygen concentration along with time and distance from oxide/substrate interface obeys the Fick's second law [7,9,39], i.e.,

$$C(x,t) = C_s\left[1 - \mathrm{erf}\left(\frac{1}{2\sqrt{Dt}}x\right)\right] \tag{21}$$

where erf$(\cdot)$ is the error function, C_s is the oxygen concentration at the oxide/alloy interface, and D and x are respectively diffusivity and depth. Then, the flux due to oxygen solution in ODZ, J_s, can be expressed as

$$J_s(t) = \int_0^{+\infty}\frac{\partial C(x,t)}{\partial t}dx = 2C_s\sqrt{\frac{D}{\pi}}t^{-0.5} \tag{22}$$

Then Eq. (15) can be rewritten as

$$\frac{d\varepsilon_g}{dt} = \begin{cases} R_{ox1}t^{\gamma_1-1} + \frac{4V_{MO_z}C_sR_{ox1}}{z\gamma_1 K_{ox1}{}^{\gamma_1}}\sqrt{\frac{D}{\pi}}t^{-0.5} & (t \le t_0) \\ R_{ox2}\left[K_{ox2}(t-t_0) + (K_{ox1}t_0)^{\frac{1}{\gamma_2}\gamma_1}\right]^{\gamma_2-1} + \frac{4V_{MO_z}C_sR_{ox2}}{z\gamma_1 K_{ox2}}\sqrt{\frac{D}{\pi}}t^{-0.5} & (t > t_0) \end{cases} \tag{23}$$

where

$$R_{ox1} = \frac{1}{2bdaV_{MO_z}} \Omega\theta A_1 z\gamma_1 K_{ox1}{}^{\gamma_1} \tag{24a}$$

$$R_{ox2} = \frac{1}{2bdaV_{MO_z}} \Omega\theta A_1 z\gamma_2 K_{ox2} \tag{24b}$$

When $t \le t_0$, the expression of growth stress rate within the oxide layer can be expressed as

$$\frac{d\sigma_g}{dt} = -\frac{E_{ox}R_{ox1}}{1-\nu_{ox}}\left[t^{\gamma_1-1} + \frac{4V_{MO_z}C_s}{z\gamma_1 K_{ox1}{}^{\gamma_1}}\sqrt{\frac{D}{\pi}}t^{-0.5} + \mathrm{sgn}(\sigma_g)\times B|\sigma_g|^m\right] \tag{25a}$$

When $t > t_0$, the growth stress rate is

$$\frac{d\sigma_g}{dt} = -\frac{E_{ox}R_{ox2}}{1-\nu_{ox}}\left\{[K_{ox2}(t-t_0) + (K_{ox1}t_0)^{\frac{1}{\gamma_2}\gamma_1}]^{\gamma_2-1} + \frac{4V_{MO_z}C_s}{z\gamma_2 K_{ox2}}\sqrt{\frac{D}{\pi}}t^{-0.5} + sgn(\sigma_g)\times B|\sigma_g|^m\right\} \tag{25b}$$

Since the creep index of rutile, m, is 1.0 [40], the growth stress in the oxide layer, σ_g, can be determined through the integration of Eq. (25). When $t \le t_0$, σ_g is expressed as

$$\sigma_g = \exp\left(-\frac{E_{ox}Bt}{1-\nu_{ox}}\right)\left\{C_1 - \int \exp\left(\frac{E_{ox}Bt}{1-\nu_{ox}}\right)\left[\frac{E_{ox}R_{ox1}}{1-\nu_{ox}}t^{\gamma-1} + \frac{4V_{MO_z}C_sR_{ox1}E_{ox}}{z\gamma_1(1-\nu_{ox})K_{ox1}{}^{\gamma_1}}\sqrt{\frac{D}{\pi}}t^{-0.5}\right]dt\right\} \tag{26}$$

Considering the series expansion of exponential function, namely

$$e^x = \sum_{n=0}^{+\infty}\frac{x^n}{n!} \tag{27}$$

Eq. (26) can be rewritten as

$$\sigma_g = \exp\left(-\frac{E_{ox}Bt}{1-\nu_{ox}}\right)\left\{C_1 - 4\sum_{n=0}^{+\infty}\left[\frac{E_{ox}{}^{n+1}B^nV_{MO_z}C_sR_{ox1}}{(1-\nu_{ox})^{n+1}(n+0.5)z\gamma_1 n!K_{ox1}{}^{\gamma_1}}\sqrt{\frac{D}{\pi}}t^{n+0.5}\right] - \sum_{n=0}^{+\infty}\left[\frac{E_{ox}{}^{n+1}B^nR_{ox_1}t^{n+\gamma}}{(1-\nu_{ox})^{n+1}(n+\gamma_1)n!}\right]\right\}$$

(28a)

$$C_1 = 12E_{ox}hy\frac{1}{(1-\nu_{ox})(3H^2-4A^2)} + \sigma_i \tag{28b}$$

where σ_i is the intrinsic growth stress. When $t \ge t_0$, σ_g is expressed as

$$\sigma_g = \exp\left(-\frac{E_{ox}Bt}{1-\nu_{ox}}\right)\left\{C_2 - 4\sum_{n=0}^{+\infty}\left[\frac{E_{ox}{}^{n+1}B^nV_{MO_z}C_sR_{ox2}}{(1-\nu_{ox})^{n+1}(n+0.5)z\gamma_2 n!K_{ox2}}\sqrt{\frac{D}{\pi}}t^{n+0.5}\right] - \sum_{n=0}^{+\infty}\left[\frac{E_{ox}{}^{n+1}B^nR_{ox_2}Q(n)}{(1-\nu_{ox})^{n+1}}\right]\right\} \tag{29a}$$

$$Q(n) = \sum_{q=0}^{n}\left\{\frac{1}{\gamma_2(\gamma_2+1)\cdots(\gamma_2+q)K_{ox2}{}^{q+1}}(-1)^q[K_{ox2}(t-t_0) + (K_{ox1}t_0)^{\frac{1}{\gamma_2}\gamma_1}]^{\gamma_2.+q}t^{n-q}\prod_{L=n-q+1}^{n}L(q)\right\} \tag{29b}$$

$$C_2 = \sigma_g(t_0)\exp\left(\frac{E_{ox}Bt_0}{1-\nu_{ox}}\right) + 4\sum_{n=0}^{+\infty}\left[\frac{E_{ox}{}^{n+1}B^nV_{MO_z}C_sR_{ox2}}{(1-\nu_{ox})^{n+1}(n+0.5)z\gamma_2 n!K_{ox2}}\sqrt{\frac{D}{\pi}}t_0{}^{n+0.5}\right] + \sum_{n=0}^{+\infty}\left[\frac{E_{ox}{}^{n+1}B^nR_{ox_2}}{(1-\nu_{ox})^{n+1}}Q(n)|_{t=t_0}\right] \tag{29c}$$

3.3. Properties of oxide

The Young's modulus and Poisson's ratio of rutile are respectively 455 GPa and 0.26 [38]. The *PBR* of titanium is set to be 2.0 ± 0.2 [41]. The CTEs of alumina, rutile and Ti-6Al–4V are respectively 7.6×10^{-6} [42], 7.7×10^{-6} [42] and $9.5\times10^{-6}\,K^{-1}$ [43]. The creep constant of rutile, B, is predicted using the following equation

$$B = B_0\exp\left(-\frac{Q}{RT}\right) \tag{30}$$

where B_0 is a constant, Q is the activation energy of creep, R is gas constant. The magnitudes of B_0 and Q of impure rutile are respectively $0.1245\,Pa^{-1}\,s^{-1}$ and $264\,kJ\,mol^{-1}$, which are determined through fitting the experimental data by Philpot et al. [40]. The experimental results indicated that the stationary creep of polycrystalline rutile was controlled by Nabarro-Herring lattice diffusion process. Therefore, the creep index remains to be 1.0 [40]. The oxygen solubility in alpha-titanium is 34 *at.* % [44,45], and the diffusivity of oxygen in Ti-6Al–4V alloy and pure titanium are respectively 8.8×10^{-13} [9] and $1.4\times10^{-13}\,cm^2\,s^{-1}$ [45] at 873 K.

4. Experimental results

4.1. XRD patterns

Fig. 5 shows the X-ray diffraction patterns at the surfaces of the oxidized Ti-6Al-V as well as pure titanium specimens under different loading conditions, where U denotes the unloaded specimen, and T and C respectively denote the tensile and compressive surfaces of the loaded specimen. Fig. 5a reveals the typical α-Ti patterns, indicating that only a little part of oxygen has been consumed to form rutile at the oxidized surfaces after 6 h. The oxygen elements are prone to dissolve into the alloy to form solid solution in alpha-phase titanium. As an alpha-phase titanium stabilizer [44,46], the absorption of oxygen promotes the transformation from beta-phase titanium into alpha-phase, therefore no diffraction peaks of beta-phase can be detected. The rutile peak at 27.44° corresponding to (110) plane appears at the oxidized surface subjected to tensile or compressive strain, indicating that the external bend-

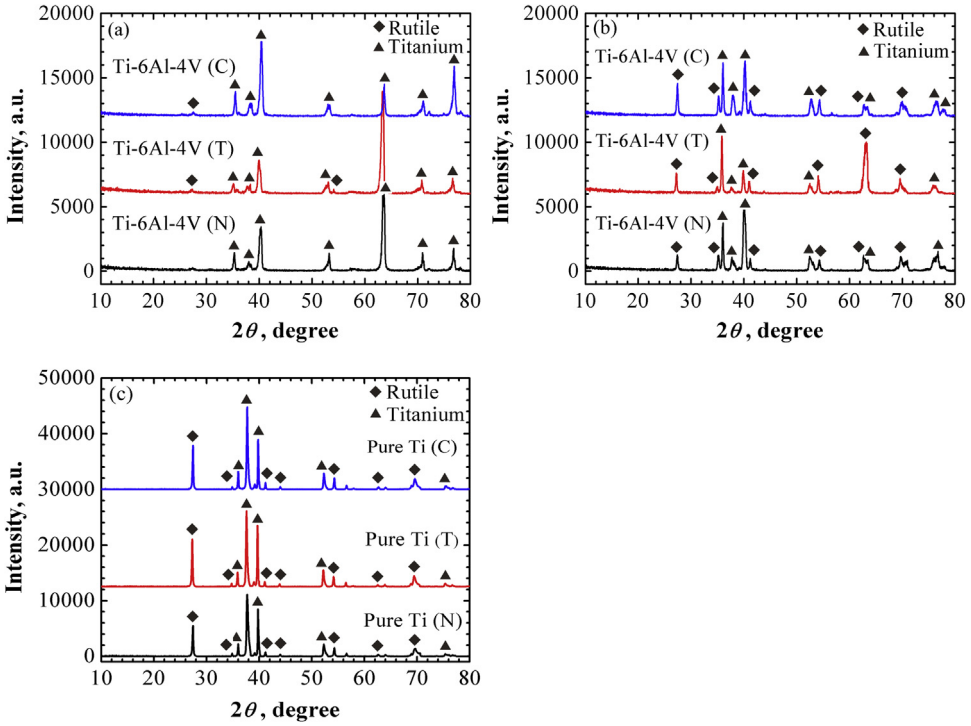

Fig. 5. XRD patterns of oxidized specimens at 873 K, (a) Ti-6Al-4V for 6hrs, (b) Ti-6Al-4V for 96 h, and (c) pure titanium for 6 h.

ing strain could promote the nucleation and formation of rutile. The XRD patterns in Fig. 5b indicate that rutile is formed after oxidation for 96 h. This phenomenon may be due to the fact that the oxygen dissolving rate decreases with increasing oxygen concentration near the interface, allowing more oxygen atoms to react with titanium to form rutile. The appearance of alpha-titanium peaks in Fig. 5b was mainly due to the penetration of X-ray beyond the oxide layer through the substrate [9]. Since the content of alumina is relatively low compared with that of rutile or titanium, alumina peaks are not found in XRD patterns, which is also confirmed by other researchers [8,9,11,47]. The XRD patterns of pure titanium are also included for comparison, as seen in Fig. 5c. The rutile and α-Ti patterns are detected at the oxidized surfaces.

It is well-known that the unit cell dimension controls the Bragg positions of the XRD peaks [37]. The solution of oxygen atoms into the substrate will lead to lattice expansion without changing the hexagonal close-packed structure (HCP) [44]. According to Eq. (2), with increasing lattice plane-spacing, Bragg diffraction angles decrease and diffraction peaks shift to the left. In Fig. 6, the α-titanium peaks corresponding to (100), (102), (110), (103) and (112) planes are selected to reflect the effect of external strain on the oxygen dissolving process, where the data were collected from Fig. 5a–c. The experimental data are fitted by using the Voigt function [37]. It can be seen that the peak-shifting takes place due to the application of external strains. For Ti-6Al–4V alloy, the tensile and compressive strains respectively lead to the shift of peaks from referential position to left and right. These results indicate that tensile and compressive strains will respectively promote and retard the diffusion of oxygen into alloy at initial stage. For pure titanium, the peaks shift to left when the tensile strains are applied. However, the effect of compressive strain on the diffusion process is not obvious.

4.2. Surface morphologies

The surface morphologies of oxidized Ti-6Al–4V alloy after oxidization for 6 and 96 h are shown in Fig. 7. As seen in Fig. 7a, the oxidized surface of unloaded specimen is relatively flat. No nodular oxide appears at the surface. While, nodular oxide has been observed at surfaces subjected to external strains, as seen in Fig. 7b and c, indicating that the external strains can accelerate the formation of oxide at the initial stage. After oxidization for 96 h, the nodular particles cover the entire surface, as seen in Fig. 7d–f. Compared with the unloaded specimen, the oxide particles on the surfaces the loaded specimen are relatively coarse and porous. Some experimental research [6–9] indicated that the outer part of the oxide was mainly composed of nodular alumina while the inner part was mainly the fine rutile. As the oxidized surface becomes more coarse and porous, the content of nodular alumina in the oxide increases due to the application of bending strains. Since the formation of alumina depends on the outward diffusion of aluminium element throughout the oxide layer, it can be concluded that the diffusion of aluminium element is promoted by the bending strains. Furthermore, the experimental results also indicate that the size of oxide particle generally increases with increasing oxidation time. The similar phenomenon was also observed by Du et al. and Kumar et al. [6,8].

Fig. 8 shows the contents of different elements at the surfaces of oxidized Ti-6Al–4V alloy after oxidation for 6 and 96 h. The contents of oxygen and aluminium generally increase while those of titanium and vanadium decreases with increasing oxidation time. The similar result can also be found in Ref. [6]. Moreover, the oxidized surface of the unloaded specimen contains a lower oxygen content compared with that of loaded specimen, indicating the formation of alumina is promoted by both tensile and compressive strains. After oxidation for 96 h, aluminium content at the surface of unloaded specimen is 3.8 wt.%. While, the aluminium contents at the tensile and compressive surfaces of the loaded specimen are respectively 6.5 wt.% and 6.0 wt.%. This result indicates that the external strains can promote the formation of alumina. When the oxide layer is patchy or non-integrated, the aluminium content in the Ti-6Al–4V alloy (around 6 wt.%) will affect the accuracy of measurement. In such a case, the aluminium content at surfaces of the specimens after oxidation time of 6 h could be overestimated. Consequently, the difference between the aluminium content after oxidation time

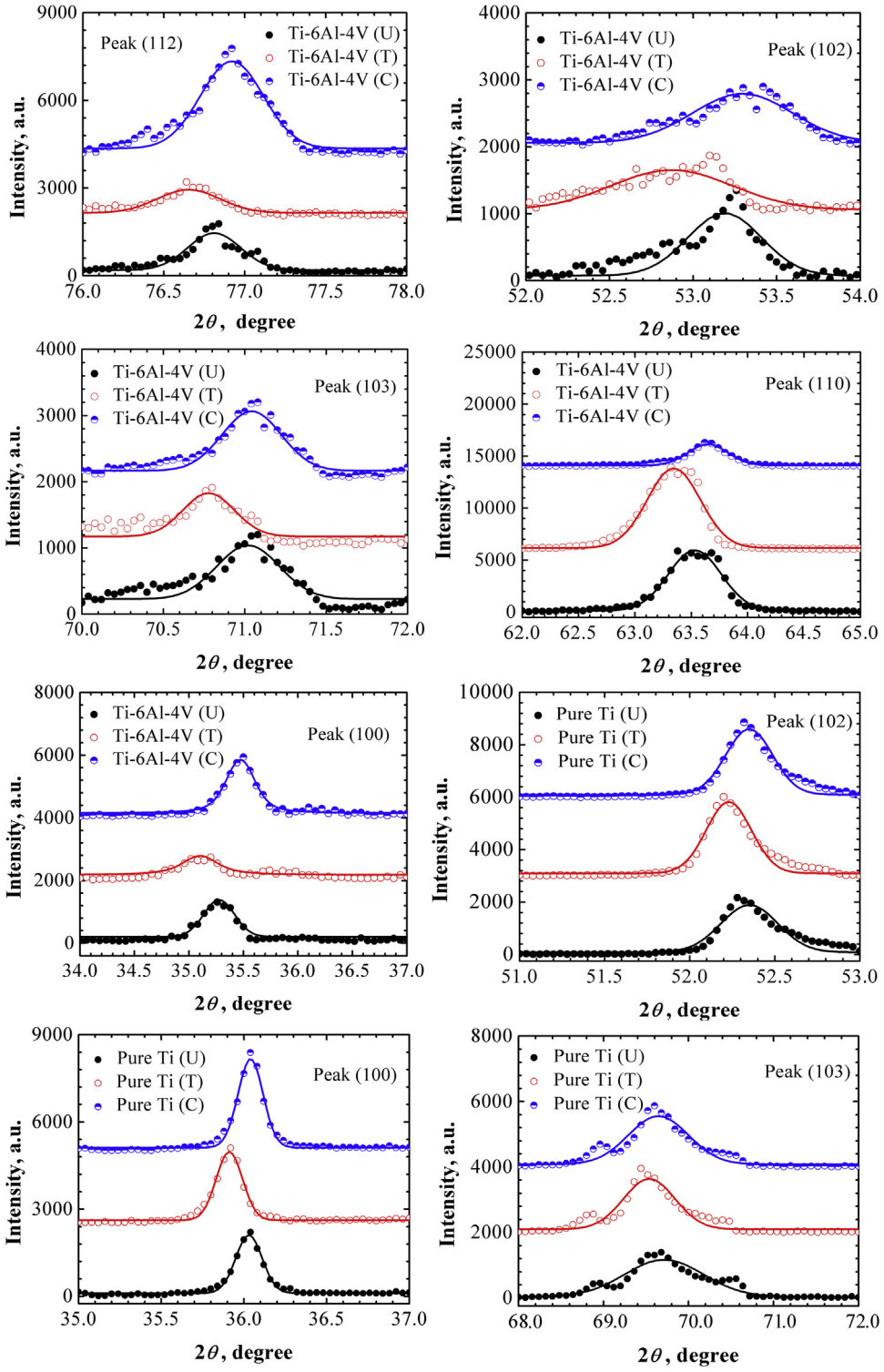

Fig. 6. XRD patterns of oxidized specimens at 873 K after 6 h. The titanium peaks corresponding to (100), (102), (110), (103) and (112) planes are selected to illustrate the effect of external strains on the oxygen solution process.

of 6 h and that at surface of unloaded specimen after 96 h cannot be distinguished. Since aluminium and titanium will compete with each other to react with oxygen, the content of titanium is negatively correlated with that of aluminium, as seen in Fig. 8. The EDS result shows that there is still small amount of residual vanadium remaining in the oxide. The formation of alumina will be prevented if there is a high content of vanadium, since vanadium will reduce the activity of aluminium [6,48]. Hence, the oxide surface with a high aluminium content generally contains a relatively lower vanadium content.

4.3. Cross-sectional morphologies

The cross-sectional morphologies of oxidized specimens after oxidation for 36 and 96 h are shown in Fig. 9. The oxide layer, ODZ and substrate can be easily distinguished. The outer part of the

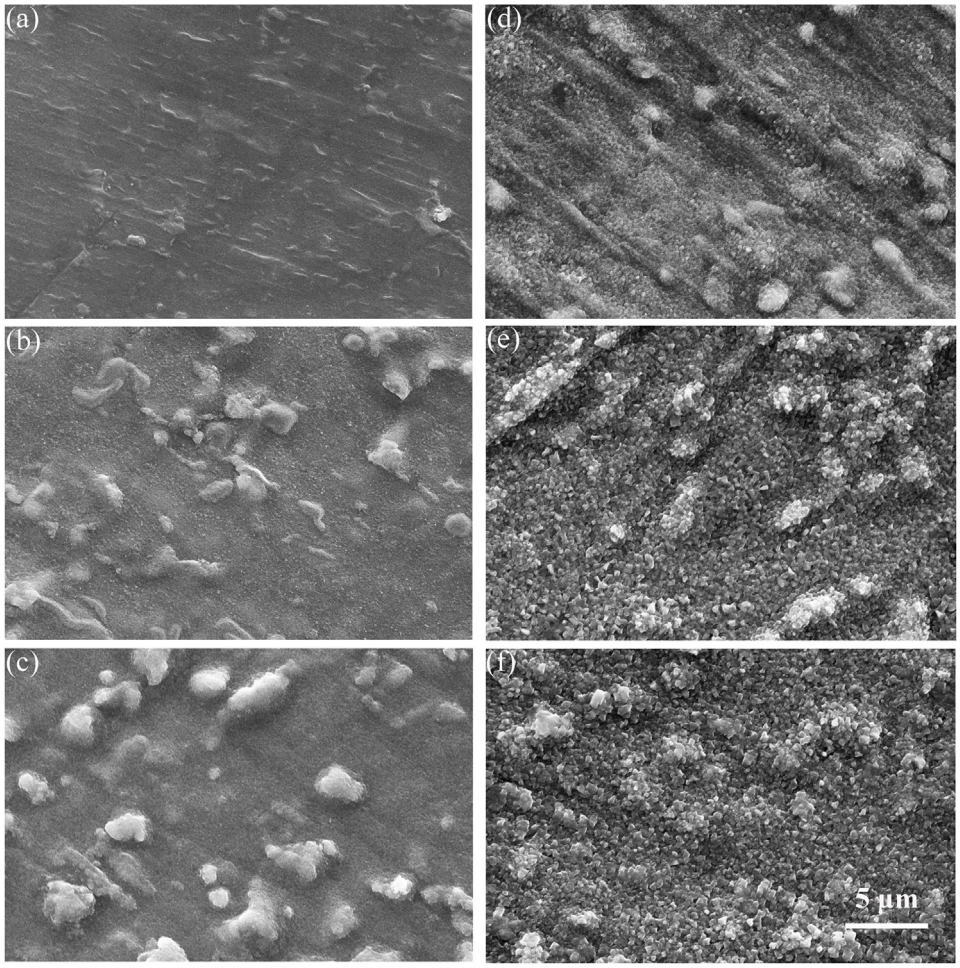

Fig. 7. Morphologies at the surfaces of unloaded specimens after oxidation time of (a) 6 h and (d) 96 h, at the surface subjected to tensile strain after oxidation time of (b) 6 h and (e) 96 h, and at the surface subjected to compressive strain after oxidation time of (c) 6 h and (f) 96 h.

oxide is coarser and more porous compared with the inner part. Meanwhile, a distinctive ODZ composed of alpha-phase titanium is formed beneath the oxide/alloy interface. Due to the solution of oxygen in the alloy, the amount of beta phase is reduced remarkably in ODZ [46,49].

Fig. 10a shows the variations of thickness of oxide layer, h_{ox}, along with oxidation time, t of different specimens. For each specimen, the thicknesses of oxide layer and ODZ are recorded at ten random locations along the lateral direction to determine the mean value and standard deviation. For Ti-6Al–4V alloy, the h_{ox}-t curve can be divided into two stages with a piecewise point of 36 h. Before the piecewise point, the thickness of oxide layer at the surface of unloaded specimen is relatively lower than that at the surface of the loaded specimen. Since rutile is the unique oxidation product in the initial stage, the experimental results indicate that the formation of rutile is promoted by both tensile and compressive strains. After the piecewise point of 36 h, the unloaded specimen shows a much faster oxidation rate. Hence, the piecewise point, t_0, in Eq. (7) is set to be 36 h. The oxidation kinetics of pure Ti at 866 K obtained by Unnam et al. is also included in Fig. 10a for comparison [45]. It should be noted that no external load was applied in Unnam et al.'s experiment. Since rutile is the unique product during the thermal oxidation of pure titanium, its oxidation kinetics obeys a parabolic law. Compared with the unloaded Ti-6Al–4V alloy, the oxidation rate of pure titanium is relatively high even though the temperature is relatively low. The fitted coefficients including K_{ox1}, K_{ox2}, γ_1 and γ_2 for Ti-6Al–4V alloy and pure titanium under different loading conditions are listed in Table 1. Fig. 10b shows the variations of thicknesses of ODZ in oxidized Ti-6Al–4V specimens under different loading conditions along with oxidation time. It is clear that the application of compressive strains will induce the deceleration of oxygen solution into the titanium alloy. However, the thickness of ODZ near the tensile surface of the loaded specimen is almost same to that near the surface of unloaded specimen. Hence, the tensile strain doesn't show an obvious influence on the formation of ODZ. According to Eq. (21), if the oxygen concentration at the ODZ bottom keeps constant, the variation of ODZ thickness along with oxidation time obeys a parabolic law, i.e.,

$$x_0 = K_{odz} t^{0.5} \tag{31}$$

where x_0 is the ODZ thickness and K_{odz} is the kinetics constant. The fitted K_{odz} is also summarized in Table 1.

Fig. 11 shows the elemental map near the surface subjected to tensile strain after 36 h. The boundaries of nickel layer are marked by two lines. It's clear that a poor aluminium region appears near the oxide/ODZ interface, indicating that outward diffusion of aluminium atoms occurs to form alumina near the gas/oxide interface. Compared with the inner part, the outer part of oxide contains a higher content of aluminium and lower content of titanium. This result reveals that the oxide is actually the mixture of rutile and alumina. Moreover, alumina grows outwards while the rutile mainly grows inwards. Although the oxide of vanadium is not favoured

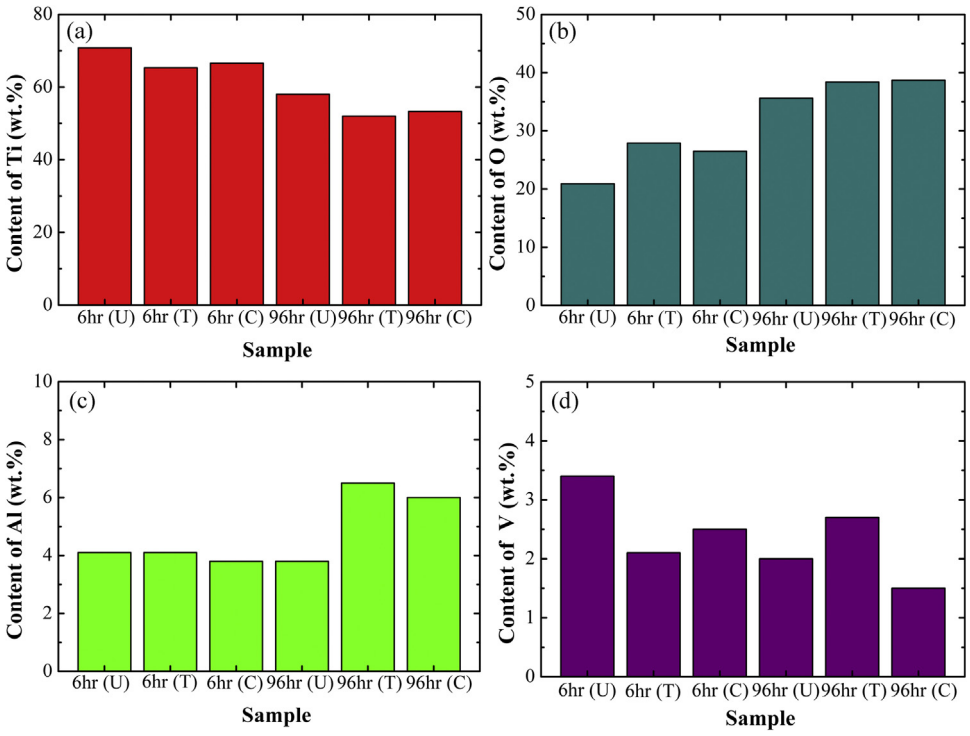

Fig. 8. Elemental contents after oxidation time of 6 and 96 h.

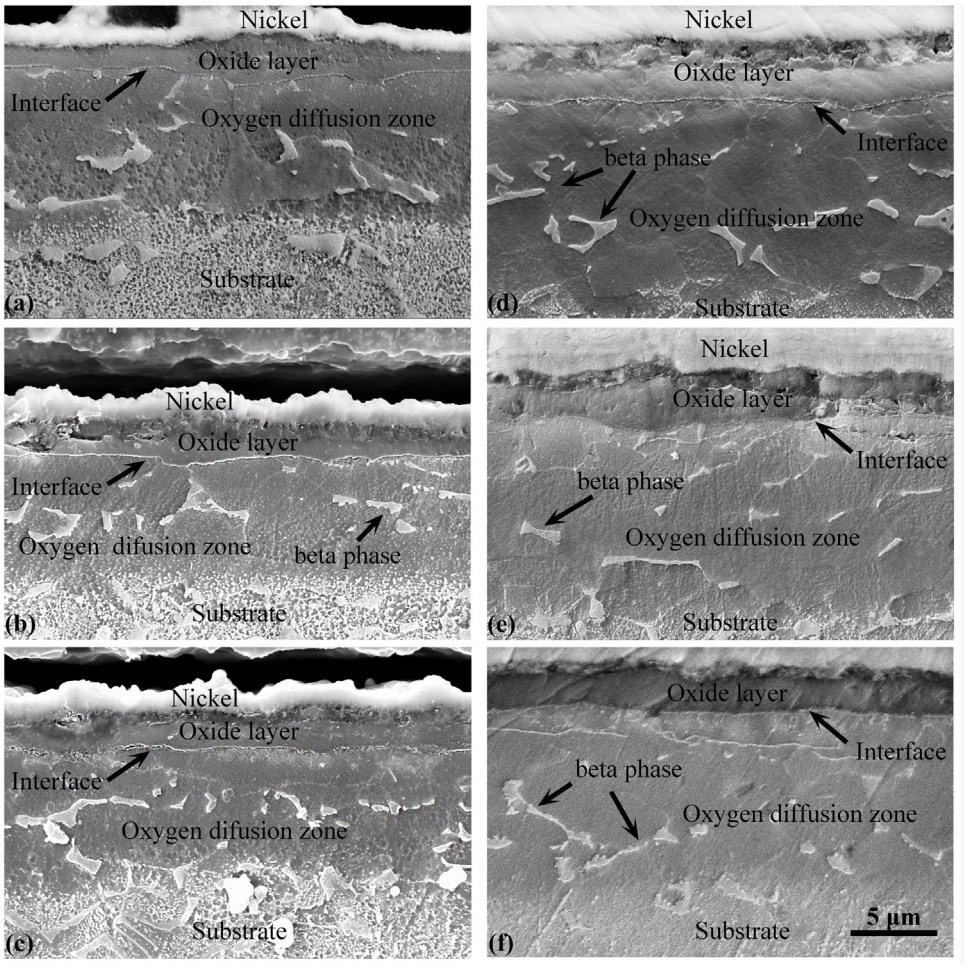

Fig. 9. Cross-sectional micrographs at the surfaces of unloaded specimens after oxidation time of (a) 36 h and (d) 96 h, at the surfaces subjected to tensile strain after oxidation time of (b) 36 h and (e) 96 h, and at the surfaces subjected to compressive strain after oxidation time of (c) 36 h and (f) 96 h.

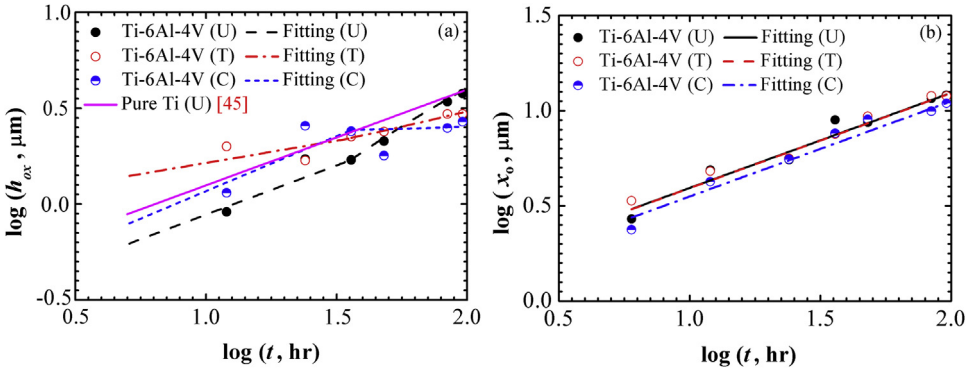

Fig. 10. Variations of (a) oxide layer thickness, and (b) ODZ thickness along with oxidation time.

Table 1
The parameters used in the calculations of growth stress.

Properties	Ti-6Al-4V(U)	Ti-6Al-4V(T)	Ti-6Al-4V(C)	Pure titanium
$K_{ox1}(m^{-\gamma_1} \cdot s^{-\gamma_1})$	4.7718×10^{-17}	2.6090×10^{-30}	1.3088×10^{-15}	4.3602×10^{-17}
γ_1	0.5134	0.2312	0.5734	0.5
$K_{ox2}(m^{-\gamma_2} \cdot s^{-\gamma_2})$	5.6162×10^{-14}	5.6548×10^{-22}	4.2152×10^{-13}	–
γ_2	0.6989	0.3523	0.9955	–
$K_{odz}(m \cdot s^{-0.5})$	2.1170×10^{-8}	2.1174×10^{-8}	1.9284×10^{-8}	–
$R_{ox1}(s^{-\gamma_1})$	-4.9298×10^{-6}	-1.2120×10^{-4}	-1.8383×10^{-6}	-1.4606×10^{-6}
$R_{ox2}(m^{(\gamma_2-1)/\gamma_2} s^{-1})$	-2.7244×10^{-11}	1.6056×10^{2}	-8.1979×10^{-19}	–
σ_i(Pa)	-1.4536×10^{9}	-2.4988×10^{9}	5.9064×10^{8}	3.7349×10^{8}

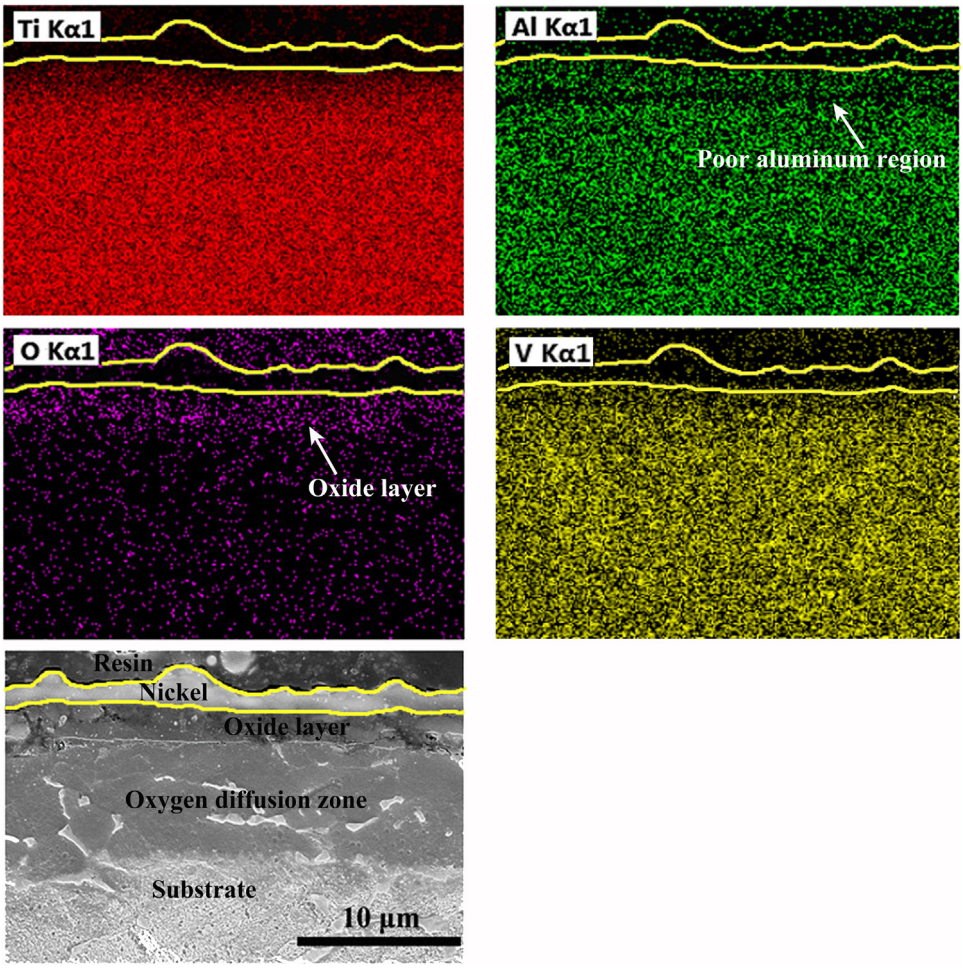

Fig. 11. Elemental map near the oxidized surface at the tensile side at oxidation time of 36 h.

during oxidation, there is still some residual vanadium detected within the oxide.

5. Discussion

5.1. Effect of external strains on oxidation behaviour

Pure rutile is formed at the surface of pure titanium through inward diffusion of oxygen and outward diffusion of titanium. However, the oxidation mechanism of Ti-6Al–4V alloy is much more complicated. In accordance with earlier investigation conclusions and present experimental results, the oxidation process of Ti-6Al–4V contains the following four steps. Firstly, as the Ti-6Al–4V alloy is exposed to oxidization environment, fine rutile nuclei are preferentially formed since activation energy for rutile is much lower than that for alumina [6]. With increasing oxidation time, the rutile nuclei will gradually cover the alloy surface [6–9], as seen in Fig. 7a. Secondly, rutile continues to form at both the gas/oxide and oxide/alloy interfaces through the outward diffusion of titanium and inward diffusion of oxygen. The addition of vanadium can effectively reduce the activity of aluminium, therefore alumina is prevented to form at the oxide/alloy interface [6,48]. Thirdly, nodular alumina begins to appear at the gas/oxide interface, as seen in Fig. 7b and c. The existence of vanadium in Ti-6Al–4V alloy reduces the solubility of aluminium and drives the aluminium to diffuse outwards. If activated-titanium atoms are insufficient at the oxide/alloy interface, aluminium atoms will be further promoted to diffuse outwards and react with oxygen. In such a case, nodular alumina becomes the preferential oxidation product at the gas/oxide interface [6,7]. Finally, the diffusivity of oxygen through the oxide layer and subsequent scale growth rate are reduced owing to the blocking effect of alumina. Meanwhile, new oxide grows in the gaps between adjacent large nodular particles, leading to the formation of mixed oxide layer composed of rutile and alumina [8], as seen in Fig. 7d–f.

From cross-sectional morphologies in Fig. 9, some defects such as small pores or cracks can be found in the vicinity of the oxide/nickel interface. However, near the oxide/ODZ interface, there are no pores or cracks observed. Since this phenomenon can be found for unloaded specimens and specimens subjected to bending strains, it can be concluded that the application of bending strains cannot change the gradient structure of the oxide layer, i.e., nodular alumina in the outer part while fine rutile in the inner part. The surface morphologies in Fig. 7 can also provided supplementary evidence to this conclusion. Fine rutile layer is formed beneath the nodular alumina. Furthermore, the elemental map in Fig. 11 shows that the contents of elements change monotonically throughout the oxide layer. The content of titanium increases while that of aluminium decreases with increasing depth from surface. This is related to the competitive relation between titanium and aluminium when reacting with oxygen. Moreover, Fig. 8 clearly shows that the formation of alumina at the surface is promoted due to the application of bending strains. Hence, it can be conclude that the external strains could promote the formation of aluminium and improve its content throughout the oxide layer.

From Fig. 10a, it is clearly found that the external strains have different effects on the oxidation behaviour of Ti-6Al–4V alloy in different oxidation stages. Before the piecewise point, i.e., 36 h, the formation of oxide are promoted by the application of bending strains, due to the reduction of required energy for the nucleation as well as growth of oxide. Under bending strains, large amount of defects including vacancies or dislocations are accumulated near the surface of Ti-6Al–4V alloy owing to creep deformation [50,51]. The existence of these defects can remarkably reduce the activation energy and promote the nucleation of fresh oxide. However, after the piecewise point, the bending strain will show a retarding effect on the oxidation process. This is attributed to the accelerated outward diffusion of aluminium and the promoted formation of nodular alumina. As mentioned above, the application of external bending strains will increase the content of alumina phase in the oxide layer, especially at the gas/oxide interface. Considering the blocking effect of alumina on the inward diffusion of oxygen, the formation of rutile will be decelerated as the oxygen flux is insufficient. Consequently, the bending strains show a retarding effect on the oxide growth in the later oxidation stage.

5.2. Effect of external strains on the formation of ODZ

At the oxide/alloy interface, part of the oxygen further dissolves into the alloy to form ODZ underneath the oxide layer. Moreover, as an alpha-phase titanium stabilizer, the absorption of oxygen also promotes the transformation from beta-phase into alpha-phase [44]. For Ti-6Al–4V alloy, the compressive strain will retard the formation of ODZ while the effect of tensile strain is not clear, as seen in Fig. 10. For pure titanium, the external strains show a distinct effect due to the disappearance of alumina in oxide. As seen in Fig. 6, the XRD peaks of alpha titanium shift to left when the tensile strain is applied, indicating the increase of dissolved-oxygen concentration near the oxide/substrate interface.

The effect of external strains on the formation of ODZ in oxidized Ti-6Al–4V alloy is multi-fold. Firstly, due to the promoted formation of alumina, the oxygen diffusion through the oxide layer is retarded, leading to the insufficiency of oxygen flux. Consequently, the absorption of oxygen will be decelerated by the application of bending strains. Secondly, the accumulation of dislocations during creep deformation will attract the dissolving oxygen atoms due to the energetic interaction between dislocation and point defect in alloys [52]. In such a case, the formation of ODZ will be accelerated by the application of bending strains. Thirdly, the direction of dislocations will affect the absorption of oxygen. The application of external bending strains will lead to the generation of edge dislocations at surfaces. However, the directions of edge dislocations at the surfaces subjected to tensile and compressive strains are opposite, as seen in Fig. 12. More positive dislocations are generated near the surface subjected to tensile strain, while more negative dislocations are generated near the surface subjected to compressive strain. As illustrated in Fig. 12, each edge dislocation has a specific stress field consisting of a tensile zone and a compressive zone. On the basis of minimum energy principle, the interstitial atoms will be driven to migrate from the compressive zone to the tensile zone within the dislocation stress field. Consequently, the ODZ under tensile strains will be thicker than that under compressive strains in a macro-scale.

5.3. Growth stress within oxide layer

Residual stress within the oxide layer is measured at room temperature, as seen in Fig. 13a. The thermal stress within the oxide layer is evaluated as −664 MPa according to Eq. (6). In order to obtain the growth stress, thermal stress should be subtracted from the measured residual stress. The experimental results of growth stress at 873.15 K are shown in Fig. 13b. According to the classical *PBR* criteria, compressive stress will be generated when value of *PBR* is higher than 1.0. However, the present experimental results indicate that tensile growth stress is generated within oxide layer, although the *PBR* value of titanium is around 2.0 [41]. The similar results were also obtained in the previous research. Tensile growth stresses were also measured in naturally grown rutile on Ti-6Al–4V alloy at room temperature [38] and in thermally grown alumina on FeCrAlY alloy at high temperature [17]. Thus, Clarke's theory seems to be more reasonable, where the dislocation climb is responsible

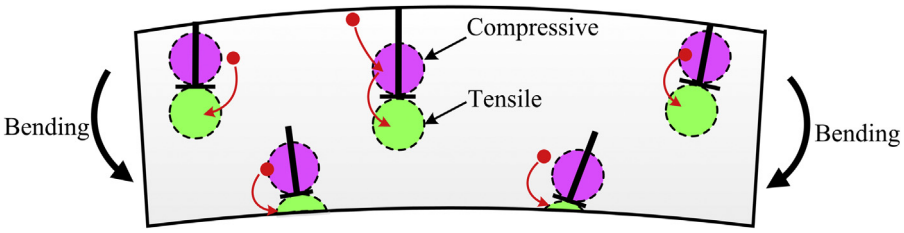

Fig. 12. Schematic showing how the stress field of edge dislocations affects the movement of oxygen atoms.

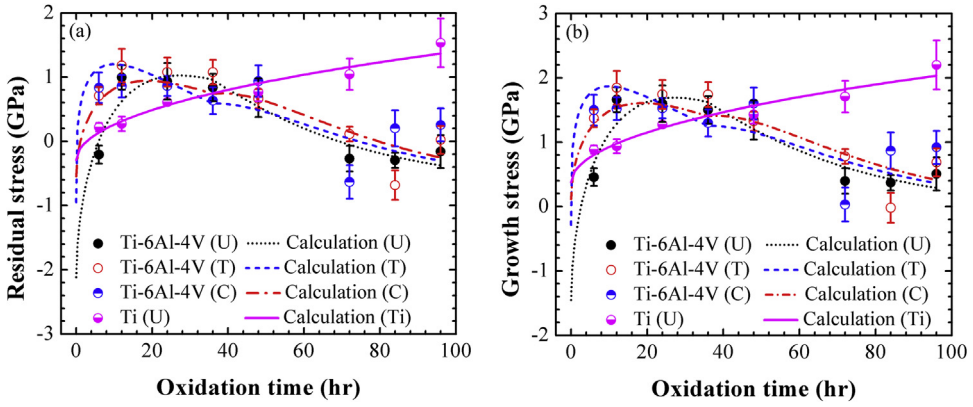

Fig. 13. The variations of (a) residual stress, and (a) growth stress within the oxidation layer Ti-6Al-4V alloy and pure titanium of along with oxidation time.

for the generation of growth strain [22]. As mentioned above, if dislocation climbs in the negative direction, tensile stress will be generated within the oxide layer.

For the case of Ti-6Al–4V alloy, the growth stress increases, reaches a local maximum, and then decreases gradually with increasing the oxidation time. The maximum values of tensile growth stresses are in the range from 1.5 to 2 GPa. The growth stress in the case of pure titanium is also included for comparison, which monotonously increases with increasing oxidation time. After oxidation for 96 h, the tensile growth stress exceeds 2 GPa. Therefore, it indicates that the addition of alloying element will accelerate the initial stress accumulation and the subsequent stress relaxation. At 6 h, the Ti-6Al–4V alloy specimen subjected to bending strains shows a larger growth stress compared with unloaded specimen, which may be due to the load assisted promotion of oxidation in the initial stage. The present analytical model is used to calculate the growth stress within the oxide. The analytical solution in the form of infinite series is given by Eqs. (28) and (29), which has to be simplified to finite series during calculation. Second-order series expansion is supposed to provide enough accuracy for calculation. However, the values of some parameters used in calculation are still difficult to measure or determine. In the present work, the fitting method through minimizing the sum of squares is employed to obtain the values of some parameters. The fitted values of R_{ox1}, R_{ox2} and σ_i are listed in Table 1. The calculated results agree well with the experimental data, as seen Fig. 13b. This model shows its advantages over earlier analytical models on the prediction of growth stress [23–27,32]. Additional component of growth strain due to the formation of ODZ and piecewise oxidation kinetics have been taken into consideration in the present model.

6. Conclusions

The following conclusions can be drawn from the present work:

1. The external tensile and compressive strains showed similar effects on the growth of oxide layer of Ti-6Al–4V. In the initial stage, dislocation was accumulated near the surface due to creep deformation, leading to the reduction of activation energy and promoted formation of rutile and alumina. However, in the later stage, the alumina phase could block the inward diffusion of oxygen and then the oxidation process was retarded.
2. For Ti-6Al–4V alloy, compressive strain would retard the formation of ODZ while the effect of tensile strain was not clear. For pure titanium, tensile strain would promote the formation of ODZ while the effect of compressive strain was not clear. The external strains showed multi-fold influences on the formation of ODZ, which was related to the blocking effect of alumina on oxygen and the interactions among dislocations and interstitial atoms.
3. An analytical model on the basis of Clarke's theory was developed to predict the growth stress within the oxide layer. The effects of ODZ and the piecewise oxidation kinetics on growth strain were taken into consideration in this mode. The predicted results by using the present model agreed well with the experimental data.

Acknowledgements

The author would like to acknowledge gratefully for the financial support through National Natural Science Foundations of China (51371082, 51322510) and 111project. The author Xian-Cheng Zhang is also grateful for the support by Shanghai Pujiang Program, Young Scholar of the Yangtze River Scholars Program, and Shanghai Technology Innovation Program of SHEITC (CXY-2015-001).

References

[1] V.A. Alves, R.Q. Reis, I.C.B. Santos, D.G. Souza, T. de, F. Goncalves, M.A. Pereira-da-Silva, A. Rossi, L.A. da Silva, *In situ* impedance spectroscopy study of the electrochemical corrosion of Ti and Ti-6Al-4V in simulated body fluid at 25 °C and 37 °C, Corros. Sci. 51 (2009) 2473–2482.
[2] R. Narayanan, S.K. Seshiadri, Phosphoric acid anodization of Ti-6Al-4V-structure and corrosion aspects, Corros. Sci. 49 (2007) 542–558.

[3] N. Dai, L. Zhang, J. Zhang, Q. Chen, M. Wu, Corrosion behaviour of selective laser melted Ti-6Al-4V alloy in NaCl solution, Corros. Sci. 102 (2016) 484–489.
[4] V.M.C.A. Oliveira, C. Aguiar, A.M. Vazquez, A. Robin, M.J.R. Barboza, Improving corrosion resistance of Ti-6Al-4V alloy through plasma-assisted PVD deposited nitride coatings, Corros. Sci. 88 (2014) 317–327.
[5] S. Lozano-Perez, K. Kruska, I. Iyenga, T. Terachi, T. Yamada, The role of cold work and applied stress on surface oxidation of 304 stainless steel, Corros. Sci. 56 (2012) 78–85.
[6] H.L. Du, P.K. Datta, D.B. Lewis, J.S. Burnell-Gray, Air oxidation behavior of Ti-6Al-4 V alloy between 650 and 850 °C, Corros. Sci. 36 (1994) 631–642.
[7] S. Frangini, A. Mignone, F. De Riccardis, Various aspects of the air oxidation behaviour of a Ti6Al4V alloy at temperatures in the range 600–700C, J. Mater. Sci. 29 (1994) 714–720.
[8] S. Kumar, T.S.N.S. Narayanan, S.G.S. Raman, S.K. Sechadri, Thermal oxidation of Ti6Al4 V alloy: microstructural and electrochemical characterization, Mater. Chem. Phys. 119 (2010) 337–346.
[9] H. Güleryüz, H. Cimenoğlu, Oxidation of Ti-6Al-4V alloy, J. Alloy Compd. 472 (2009) 241–246.
[10] M. Chen, W. Li, M. Shen, S. Zhu, F. Wang, Glass-ceramic coating on titanium alloys for high temperature oxidation protection: oxidation kinetics and microstructure, Corros. Sci. 74 (2013) 178–186.
[11] H. Güleryüz, H. Cimenoğlu, Surface modification of a Ti-6Al-4V alloy by thermal oxidation, Surf. Coat. Technol. 192 (2005) 164–170.
[12] D.W. McKee, S.C. Huang, The oxidation behaviour of gamma-titanium aluminide alloys under thermal cycling conditions, Corros. Sci. 33 (1992) 1899–1914.
[13] H. Dong, X.Y. Li, Oxygen boost diffusion for the deep-case hardening of titanium alloys, Mater. Sci. Eng. A280 (2000) 303–310.
[14] M. Wen, C. Wen, P. Hodgson, Y. Li, Thermal oxidation behaviour of bulk titanium with nanocrystalline surface layer, Corros. Sci. 59 (2012) 352–359.
[15] Y. Wouters, L. Marchetti, A. Galerie, J.P. Petit, Photoelectrochemical imaging of metal-scale decohesion on titanium thermally oxidised in oxygen, Corros. Sci. 50 (2008) 1122–1131.
[16] V.K. Tolpygo, J.R. Dryden, D.R. Clarke, Determination of the growth stress and strain in α-Al2O3 scales during the oxidation of Fe-22Cr-4.8Al-0.3Y alloy, Acta Mater. 46 (1998) 927–937.
[17] B.W. Veal, A.P. Paulikas, P.Y. Hou, Tensile stress and creep in thermally grown oxide, Nat. Mater. 5 (2006) 349–351.
[18] A.M. Huntz, Stresses in NiO, Cr_2O_3 and Al_2O_3 oxide scales, Mater. Sci. Eng. A201 (1995) 211–228.
[19] M. Kemdehoundja, J.L. Grosseau-Poussard, J.F. Dinhut, Growth stresses in α-Cr_2O_3 thermal oxide films determined by in situ high temperature Raman spectroscopy, J. Appl. Phys. 102 (2007) 093513.
[20] H.E. Evans, Stress effect in high temperature oxidation, Int. Mater. Rev. 40 (1995) 1–40.
[21] B. Pieraggi, R.A. Rapp, J.P. Hirth, Role of interface structure and interfacial defects in oxide scale growth, Oxid. Met. 44 (1995) 63–79.
[22] D.R. Clarke, The lateral growth strain accompanying the formation of a thermally grown oxide, Acta Mater. 51 (2003) 1393–1407.
[23] Y. Zhang, X.C. Zhang, S.T. Tu, Coupled mechanical-oxidation modelling during silicon thermal oxidation process, AIP Adv. 5 (2015) 097105.
[24] S. Maharjan, X.C. Zhang, Z.D. Wang, Analytical modeling of stress and strain of symmetrically oxidized metal, J. Appl. Phys. 112 (2012) 033514.
[25] S. Maharjan, X.C. Zhang, F.Z. Xuan, Z.D. Wang, S.T. Tu, Residual stresses within oxide layers due to lateral growth strain and creep strain: analytical modelling, J. Appl. Phys. 110 (2011) 063511.
[26] J.L. Ruan, Y.M. Pei, D.N. Fang, On the elastic and creep stress analysis modeling in the oxide scale/metal substrate system due to oxidation growth strain, Corros. Sci. 66 (2013) 315–323.
[27] Y. Suo, S. Shen, General approach on chemistry and stress coupling effects during oxidation, J. Appl. Phys. 114 (2013) 164905.
[28] G. Moulin, P. Aervalo, A. Salleo, Influence of external mechanical loadings (creep, fatigue) on oxygen diffusion during nickel oxidation, Oxid. Met. 45 (1995) 153–181.
[29] Md. Zafir Alam, K. Dipak Das, Effect of cracking in diffusion aluminide coating on their cyclic oxidation performance on Ti-based IMI-834 alloy, Corros. Sci. 51 (2009) 1405–1412.
[30] A. Fargeix, G. Ghibaudo, Dry oxidation of silicon: a new model of growth including relaxation of stresses by viscous flow, J. Appl. Phys. 54 (1983) 7153.
[31] G. Zumpicchiat, S. Pascal, M. Tupin, C. Berdin-Méric, Finite element modelling of the oxidation kinetics of Zircaloy-4 with a controlled metal-oxide interface and the influence of growth stress, Corros. Sci. 100 (2015) 209–221.
[32] Y. Zhang, X.C. Zhang, S.T. Tu, F.Z. Xuan, Analytical modeling on stress assisted oxidation and its effect on creep response of metals, Oxid. Met. 82 (2014) 311–330.
[33] E.A. Irene, Silicon oxidation studies: a revised model for thermal oxidation, J. Appl. Phys. 54 (1983) 5416–5420.
[34] C.H. Zhou, H.T. Ma, L. Wang, Comparative study of oxidation kinetics for pure nickel oxidized under tensile and compressive stress, Corros. Sci. 52 (2010) 210–215.
[35] G.E. Pellissier, S.M. Purdy, Stereology and Quantitative Metallography, American Society for Testing and Materials, Atlantic City, 1971.
[36] Standard practice for preparation and use of bent-beam stress-corrosion testspecimens, ASTM G39-99. http://www.astm.org/Standards/G39.htm.
[37] U. Welzel, J. Ligot, P. Lamparter, A.C. Vermeulen, E.J. Mittemeijer, Stress analysis of polycrystalline thin films and surface regions by X-ray diffraction, J. Appl. Crystallogr. 38 (2005) 1–29.
[38] M. Härting, G. Fritsch, Determination of the residual stress state in a natural titanium oxide layer, Acta Mater. 44 (1996) 487–492.
[39] M. Göbel, V.A.C. Haanappel, M.F. Stroosnijder, On the determination of diffusion coefficients of oxygen in one-phase Ti (α-Ti) and two-phase Ti-4Nb (α- and β-Ti) by micro-hardness measurements, Oxid. Met. 55 (2001) 137–151.
[40] K.A. Philpot, Y. Ikuma, G.R. Miller, R.S. Gordon, High temperature steady-state creep of polycrystalline rutile, pure and doped with tantalum, J. Mater. Sci. 18 (1983) 1698–1708.
[41] T.H. Teh, A. Berkani, S. Mato, P. Skeldon, G.E. Thompson, H. Habazaki, K. Shimizu, Initial stages of plasma electrolytic oxidation of titanium, Corros. Sci. 45 (2003) 2757–2768.
[42] O.J. Whittemore, N.N. Ault, Thermal expansion of various ceramic materials to 1500 °C, J. Am. Ceram. Soc. 39 (1956) 443–444.
[43] J.W. Elmer, T.A. Palmer, S.S. Babu, E.D. Specht, In situ observations of lattice expansion and transformation rates of α and β phases in Ti-6Al-4V, Mater. Sci. Eng. A391 (2005) 104–113.
[44] W.L. Wasz, F.R. Brotzen, R.B. Mclellan, A.J. Griffin, Effect of oxygen and hydrogen on mechanical properties of commercial purity titanium, Int. Mater. Rev. 41 (1996) 1–12.
[45] J. Unnam, R.N. Shenoy, R.K. Clark, Oxidation of commercial purity titanium, Oxid. Met. 26 (1986) 231–252.
[46] H. Dong, T. Bell, Enhanced wear resistance of titanium surfaces by a new thermal oxidation treatment, Wear 238 (2000) 131–137.
[47] A. Biswas, J.D. Majumdar, Surface characterization of mechanical property evaluation of thermally oxidized Ti-6Al-4V, Mater. Charact. 60 (2009) 513–518.
[48] R.A. Perkins, K.T. Chiang, Formation of alumina on Ti-Al alloys, Scr. Metall. 21 (1987) 1505–1510.
[49] G. Welsch, W. Bunk, Deformation modes of the α-phase of Ti-6Al-4V as a function of oxygen concentration and aging temperature, Metall. Trans. A13 (1982) 889–899.
[50] M.J.R. Barboza, C.M. Neto, C.R.M. Silva, Creep mechanisms and physical modeling for Ti-6Al-4 V, Mater. Sci. Eng. A369 (2004) 201–209.
[51] M.J.R. Barboza, E.A.C. Perez, M.M. Mederios, D.A.P. Reis, M.C.A. Nono, F.P. Neto, C.R.M. Silva, Creep behavior of Ti-6Al-4V and a comparison with titanium matrix composites, Mater. Sci. Eng. A428 (2006) 319–326.
[52] F.C. Frank, Dislocations and point defects, Discuss. Faraday Soc. 23 (1957) 122–127.